NOTES AND CORRESPONDENCE

Characterizing Midlatitude Jet Variability: Lessons from a Simple GCM

JOHN C. FYFE

Canadian Centre for Climate Modelling and Analysis, Meteorological Service of Canada, Victoria, British Columbia, Canada

DAVID J. LORENZ

Department of Atmospheric Sciences, University of Washington, Seattle, Washington

(Manuscript received 29 December 2003, in final form 25 February 2005)

ABSTRACT

Fluctuations in the tropospheric zonal jet are often characterized using anomaly patterns, or empirical orthogonal functions, representing deviations of the zonal-mean flow from climatology. In previous studies the leading anomaly pattern has been interpreted as representing north–south jet movements, while the second anomaly pattern has been interpreted as representing independent fluctuations in jet strength and width. Here it is shown that these leading anomaly patterns are in fact dependent and *together* represent north–south movements of the jet. Fluctuations in jet strength, which are approximately inversely proportional to jet width, superimpose upon these dominant north–south meanderings. The distinction between the usual anomaly pattern perspective and this new perspective may have important implications in the interpretation of tropospheric zonal jet variability.

1. Introduction

Fluctuations in the tropospheric zonal jet may be characterized using anomaly patterns, or empirical orthogonal functions (EOFs), representing the deviation of the zonal flow from climatology. The principal component time series (PCs) associated with these spatial patterns are linearly independent (i.e., uncorrelated) and are ranked according to the temporal variance that they explain. The leading anomaly pattern explains more temporal variance than the lesser patterns, and as such is usually emphasized. For example, Lorenz and Hartmann (2001) consider the leading anomaly pattern of Southern Hemisphere zonal-mean zonal wind, which they interpret as representing north–south movements of the midlatitude jet. Baroclinic eddies tend to reinforce these movements, while external Rossby waves tend to dampen them. In Lorenz and Hartmann (2001), as in many other studies employing the anomaly pattern approach, it is tacitly assumed that because of its PCs linear independence from the other PCs the leading anomaly pattern is a distinct, fundamental, mode of variability. It is that assumption that we scrutinize here using a simple global climate model (GCM) and observations.

The potential for dependence between anomaly patterns can be seen as follows. Suppose that north–south movements in the midlatitude jet are the only type of variability, then $u(\phi, t) = U[\phi - \delta(t)]$ where $U(\phi)$ is the meridional profile of the zonal jet and $\delta(t)$ is the jet position as a function of time. Taylor series expansion yields $u(\phi, t) = U(\phi) - U'(\phi)\delta + (1/2)U''(\phi)\delta^2 + \cdots$, where the primes denote ϕ differentiation. The time mean is $\overline{u(\phi, t)} = U(\phi) - U'(\phi)\overline{\delta} + (1/2)U''(\phi)\overline{\delta^2} + \cdots$, where the overbars denote time averaging. Thus anomalous $u(\phi, t)$ is given by $u(\phi, t) - \overline{u(\phi, t)} = -U'(\phi)\delta + \frac{1}{2}U''(\phi)(\delta^2 - \overline{\delta^2}) + \cdots$, (where the ϕ origin has been shifted so that $\overline{\delta} = 0$). In this expansion at least two fixed patterns—$U'(\phi)$ and $U''(\phi)$ are required to describe the anomalies. In addition, their temporal coefficients $\alpha_1(t) \equiv \delta(t)$ and $\alpha_2(t) \equiv \delta(t)^2 - \overline{\delta(t)^2}$ are functionally related by $\alpha_2 = \alpha_1^2 - \overline{\delta^2}$. Thus a scatterplot of $\alpha_1(t)$ and $\alpha_2(t)$ in 2D phase space traces out a parabolic

Corresponding author address: Dr. J. C. Fyfe, Canadian Centre for Climate Modelling and Analysis, University of Victoria, PO Box 1700, Victoria, BC, V8W 2Y2, Canada.
E-mail: John.Fyfe@ec.gc.ca

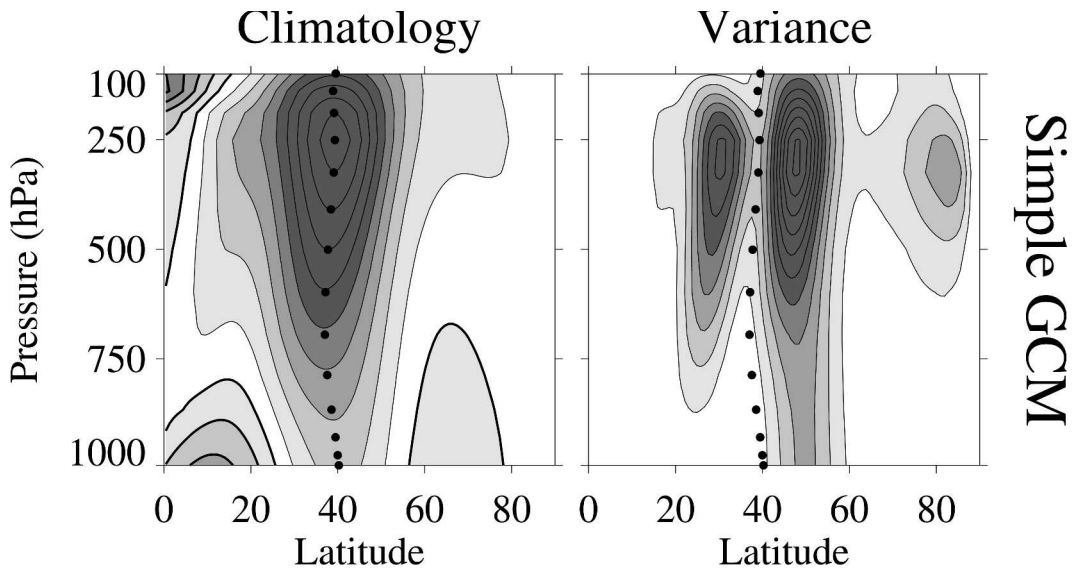

FIG. 1. (left) Climatological zonal-mean zonal wind with 4 m s^{-1} contours (. . . , −6, −2, 2, . . .). (right) Daily variance with 4 m^2 s^{-2} contours (4, 8, . . .). Thick contours are negative. The jet axis is indicated by the solid dots.

"smile"-shaped curve. In short, the leading anomaly patterns of a shifting, but otherwise constant jet profile are functionally dependent.

2. Data and methods

The simulated data used in this study are from a simple GCM. Note that we are not attempting to simulate the observed climate using the GCM. Instead, we want to begin our study of jet variability in an idealized zonally symmetric setting. The GCM is the dynamical core of the National Center for Atmospheric Research (NCAR) Community Climate Model version 3.6. The model has a T42 horizontal resolution with 28 vertical levels, and is forced by Newtonian heating and damped by Rayleigh friction in the same way as Held and Suarez (1994) except that perpetual solstice rather than perpetual equinox conditions are prescribed. This is done by changing the $\sin^2\phi$ and $\cos^2\phi$ in their $T_{\rm eq}$ formula to $0.75\sin^2\phi + 0.25\sin\phi$ and $0.75\cos^2\phi - 0.25\sin\phi$, respectively. The model is dry with no topography or zonally asymmetric heat sources. There is biharmonic diffusion on vorticity, divergence, and temperature, and regular diffusion in the top three levels to reduce the reflection of upward propagating waves. Figure 1 shows the time mean and daily variance of the simulated zonal-mean zonal wind in the winter hemisphere from a 20-yr integration of the simple GCM. The time-mean jet axis is located around 38°, with variance maxima within 15° north and south.

The observed data used in the study are from the National Centers for Environmental Prediction (NCEP)–NCAR reanalyses (Kalnay et al. 1996). We consider Southern Hemisphere (SH) data in both summer (November–March) and winter (May–September) for the years 1958–2003.

We consider daily profiles of 500-hPa zonal-mean zonal wind, $u(\phi, t)$. Anomalies of $u(\phi, t)$ are defined as $u(\phi, t) - \overline{u(\phi, t)}$ where $\overline{u(\phi, t)}$ is the daily climatology. The anomalies are weighted by the square root of the cosine of latitude (so equal areas are afforded equal weight) and EOFs computed; that is, the weighted anomalies are written as $\Sigma_n \alpha_n(t) e_n(\phi)$ where the time series $\alpha_n(t)$ are uncorrelated and the spatial patterns $e_n(\phi)$ are orthogonal. This procedure is as in Lorenz and Hartmann (2001, 2003). To help in the interpretation of the leading EOFs we also consider $u(\phi, t)$ approximated by $S\exp[-(\phi - \delta)^2/(2W)^2]$, where $S(t)$, $\delta(t)$, and $W(t)$ are the jet's strength, position, and width (obtained to very good approximation using a standard numerical technique; Marquardt 1963). This procedure is as in Fyfe (2003) for the case of NH and SH winter zonal-mean zonal wind.

3. Results

a. Simulated jet variability

Figure 2 shows a striking example of dependence between anomaly patterns. The anomaly patterns are shown in the top right-hand panel, while their associ-

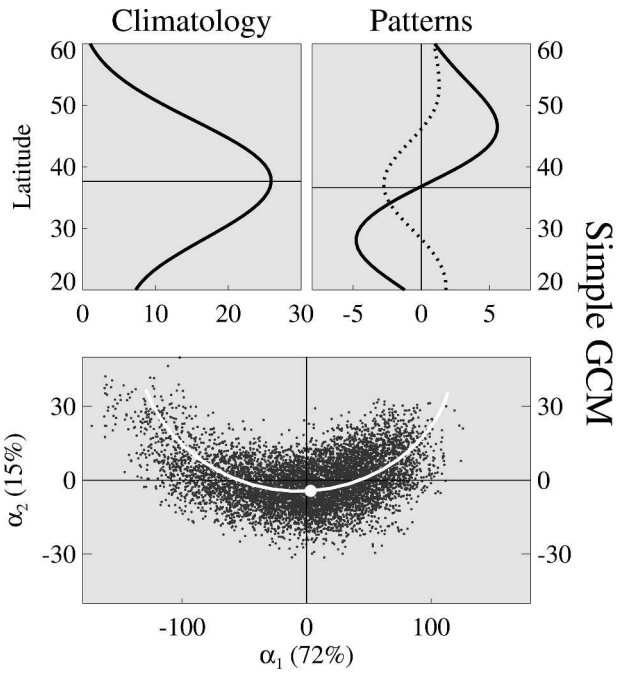

FIG. 2. EOF decomposition of the simulated 500-hPa data. (top left) Time-mean jet; units: m s^{-1}. (top right) First and second EOFs (solid and dashed curves respectively); units: m s^{-1}. (bottom) Leading PCs with percentage variance explained in the axes labels. The white curve is the linear combination of the PCs explaining pure north–south movements of the most-likely jet. The most-likely jet corresponds to the maximum of an estimate of the joint α_1 and α_2 probability distribution function (large white dot).

ated time series $\alpha_1(t)$ and $\alpha_2(t)$ are shown as the scatter of points in the bottom panel. The leading anomaly patterns are clearly dependent, given that large absolute values of $\alpha_1(t)$ are accompanied by large positive values of $\alpha_2(t)$ (i.e., giving the smile shape to the scatter of points). To help understand this dependence, consider the combination of anomaly patterns that best represents pure north–south movements of the most-likely jet profile, $U(\phi)$. The most-likely jet profile is associated with the peak in an estimate of the joint $\alpha_1(t)$ and $\alpha_2(t)$ probability distribution function (see the large white dot in Fig. 2, bottom panel). Anomalies that accompany north–south movements of the most-likely jet profile are $U(\phi - \delta) - \overline{u(\phi, t)}$, where δ is the meridional displacement of the most-likely jet profile. Projecting these anomalies onto the EOF space for a range of δ defines the white curve. The white curve passes through the scatter of points, and as such leads to the following interpretation: 1) pure north–south jet movements dominate the variability but 2) more than one anomaly pattern is required for those movements to be resolved. Not unexpectedly the larger the shift the greater the involvement of the second anomaly pattern. These results are consistent with the earlier Taylor series analysis.

It is worth reiterating that the most-likely jet profile does not correspond to the time-mean profile. Instead, the most-likely jet profile is stronger and narrower than the time-mean profile. Specifically, the maximum and width of the most-likely (time mean) profile are 28 m s^{-1} (26 m s^{-1}) and 9.0° (9.5°). In a similar fashion Swanson (2001) concludes that the observed time-mean potential vorticity (PV) profile is not a good representation of the background PV profile because of the spatial smoothing associated with time averaging.

Figure 3 provides additional help in interpreting the leading anomaly patterns. Figure 3 (left) shows $\alpha_1(t)$ and $\alpha_2(t)$ conditioned on whether the jet strength is greater than (red dots) or less than (blue dots) the most-likely jet strength. Points in the lower (upper) half of the scatter correspond to zonal jets that are stronger (weaker) than usual. Similarly, Fig. 3 (right) shows $\alpha_1(t)$ and $\alpha_2(t)$ conditioned on whether the jet latitude is greater than (red dots) or less than (blue dots) the most-likely jet position. Points in the right (left) half of the scatter corresponds to zonal jets that are more northward (southward) than usual. From here we see that a state with $|\alpha_1| \gg 0$ and $\alpha_2 = 0$ corresponds to both a shifted *and* a stronger jet. In summary, the leading anomaly patterns of $u(\phi, t)$ together describe north–south shifts of the jet, while fluctuations in jet strength superimpose upon these dominant north–south meanderings. We also conclude that interpreting the leading anomaly pattern as representing *pure* north–south movements, as in Lorenz and Hartmann (2001), would be misleading in this case.

More importantly, we conclude that the leading anomaly patterns are statistically dependent because the scatterplot of their PC time series traces out a smile-

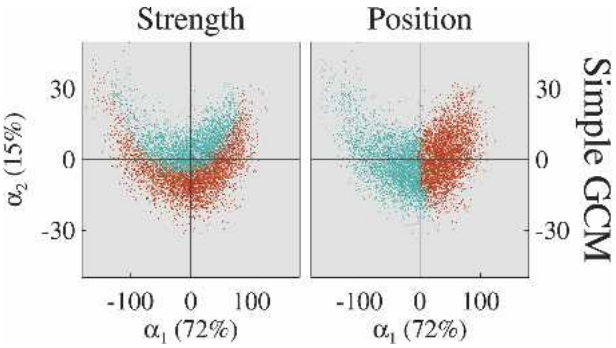

FIG. 3. PCs of the simulated 500-hPa data. (left) PCs conditioned on whether the jet strength is greater-than (red dots) or less-than (blue dots) the most-likely jet strength. (right) PCs conditioned on whether the jet position is greater-than (red dots) or less-than (blue dots) the most-likely jet position.

shaped curve in their 2D phase space. Thus, the anomaly patterns do not represent distinct, fundamental modes of variability in this case. Finally, it is useful to consider 2D scatterplots of the jet parameters themselves. Figure 4 shows jet strength versus jet position (left), as well as jet strength verses the reciprocal of jet width (right). Here we see that jet strength and position are linearly uncorrelated, while the jet strength and reciprocal width are approximately proportional (as to be expected given angular momentum conservation). Unlike the anomaly pattern case, the variability in the jet position appears to be statistically independent and therefore distinct from the other types of variability.

The distinction between the historical anomaly pattern perspective and the shifting jet perspective may have important implications in the interpretation of the midlatitude jet variability. For example, if the variability were best characterized by a zonal wind dipole pattern rather than a jet shift, then one might hypothesize that changes in the sign of the meridional shear across the time-mean jet give a fundamental description of the dynamics. Given this perspective one might then study the affects of barotropic shear on baroclinic waves in order to understand the dynamics (e.g., Thorncroft et al. 1993; Hartmann and Zuercher 1998). Because the variability is best described by a shift in the position of the midlatitude jet, however, one might look to the work of Panetta (1993) on the meridional wandering of zonal jets in wide baroclinic zones in order to gain dynamical insight.

b. Observed jet variability

Figure 5 (top right) shows the observed SH summertime anomaly patterns. These patterns are similar in structure to their simulated counterparts. In terms of magnitude, however, the second pattern takes on more relative importance in the observations than in the simulation. Figure 5 (bottom) shows the observed $\alpha_1(t)$ and $\alpha_2(t)$ scatter. First we note that the leading anomaly pattern explains much less variance than in the simulation (47% verses 72%), while the second anomaly pattern explains much more variance (29% verses 15%). Next we see in the white curve that a superposition of leading anomaly patterns is required to explain pure north–south movements of the most-likely jet profile. The fact that the white curve traces out only a hint of a smile shape in the observed scatter suggests that variability modes other than those describing pure north–south shifts are more significantly involved. We additionally note that the wintertime data behave similarly (not shown).

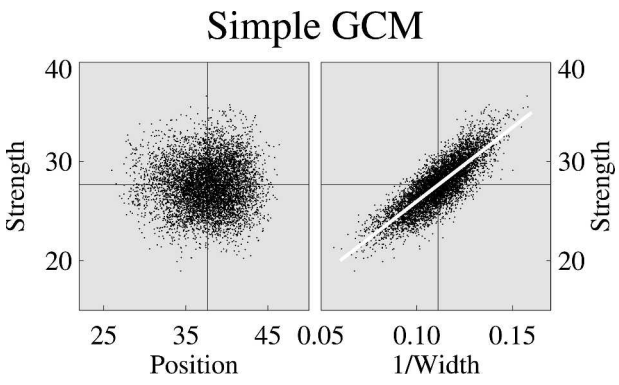

FIG. 4. Jet parameters of simulated 500-hPa data. Jet strength vs (left) position and (right) reciprocal width. Jet strength units: m s^{-1}. Jet position and width units: degrees. The white line in the left panel is the best linear fit to the scatter.

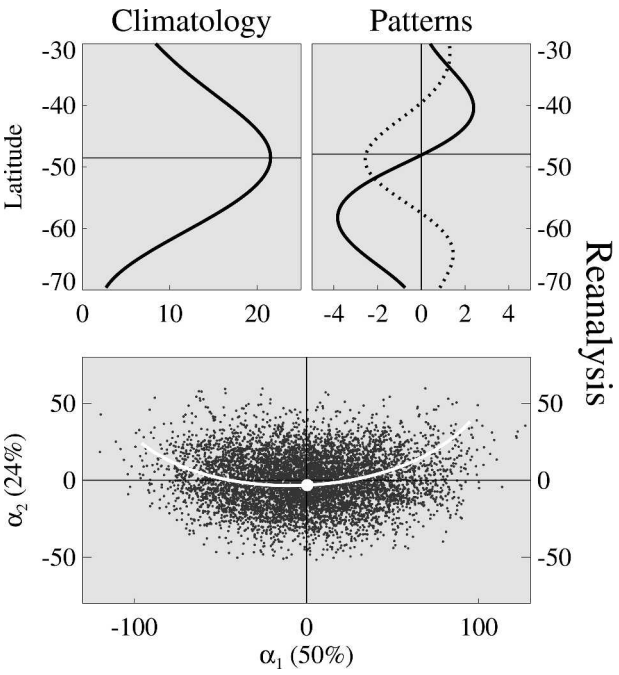

FIG. 5. As in Fig. 2, but for the SH summertime reanalysis data.

Figure 6 shows that the conditional scatterplots for the observations. If the leading anomaly pattern truly represented pure north–south movements then the distribution of red and blue points would be quite different. Specifically, in the left panel all the red points would appear below, and all blue points above, the α_2 axis. We note that as in the simple GCM a state with $|\alpha_1| \gg 0$ and $\alpha_2 = 0$ corresponds to both a shifted *and* a stronger jet. From here we conclude that the simple shifting interpretation of the leading anomaly pattern is inappropriate especially for the large shifts of the jet. Interestingly, if we artificially suppress all but shifting fluctuations a clear smile-shaped structure appears in

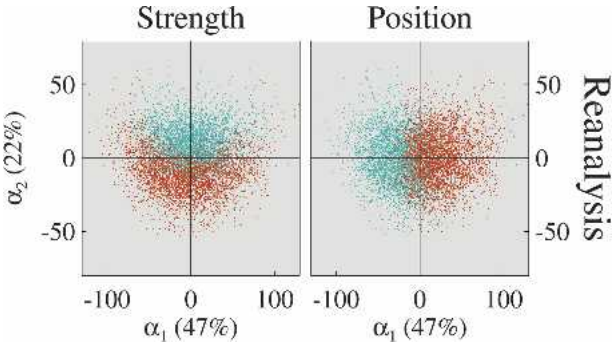

FIG. 6. As in Fig. 3, but for the SH summertime reanalysis data.

the observed scatter (not shown). Finally, we note that as in the GCM the observed jet strength and position are linearly uncorrelated, while the jet strength and reciprocal width are approximately proportional (not shown).

4. Conclusions and discussion

This paper shows that for the variability of the tropospheric zonal-mean jet, the anomaly patterns, or EOFs, showing the deviation of the flow from climatology are statistically dependent. By considering a jet profile with variable strength, position, and width we show that the leading anomaly patterns taken *together* represent north–south shifts of the jet. Fluctuations in jet strength and width superimpose upon these dominant north–south meanderings.

In addition, the results of this paper have important implications in annular mode dynamics. In both the simple GCM and observations the leading EOF of zonal wind is basically equivalent to the annular mode. In the simple GCM, other types of zonal-mean variability are particularly weak compared to the annular mode. In this simple setting, the true nature of annular mode variability (i.e., EOF1 of the zonal-mean flow) becomes apparent. The current description of the annular mode in the literature holds that the annular mode is a *fixed* anomaly pattern. This paper challenges that interpretation by stating that the annular mode is a north–south shift in the midlatitude jet, which requires more than one anomaly pattern in order to be resolved. The distinction between these two paradigms cannot be seen as clearly in the observations because the annular variability is masked by other patterns of variability.

Because annular mode variability is best described by a jet shift rather than a fixed anomaly pattern one might look to the work of Panetta (1993) on the meridional wandering of zonal jets in wide baroclinic zones in order to gain dynamical insight. The relevance of Panetta's (1993) work to our results is also supported by the variance maximum in the zonal wind near the pole (see Fig. 1, right), which corresponds to the appearance of a secondary jet in the high latitudes when the primary jet is displaced toward the equator. Thus it appears that this GCM is on the verge of producing two eddy-driven jets.

Acknowledgments. The authors are grateful to George Boer, Virginie Lorant, Adam Monahan, and Ian Watterson for their comments on an initial draft of the paper. DJL was supported by NSF grant ATM-9873691 from the Climate Dynamics Program, Atmospheric Sciences Division.

REFERENCES

Fyfe, J. C., 2003: Separating extratropical zonal wind variability and mean change. *J. Climate,* **16,** 863–874.

Hartmann, D. L., and P. Zuercher, 1998: Response of baroclinic life cycles to barotropic shear. *J. Atmos. Sci.,* **55,** 297–313.

Held, I. M., and M. J. Suarez, 1994: A proposal for the intercomparison of dynamical cores of atmospheric general circulation models. *Bull. Amer. Meteor. Soc.,* **75,** 1825–1830.

Kalnay, E., and Coauthors, 1996: The NCEP/NCAR 40-Year Reanalysis Project. *Bull. Amer. Meteor. Soc.,* **77,** 437–471.

Lorenz, D. J., and D. L. Hartmann, 2001: Eddy-zonal flow feedback in the Southern Hemisphere. *J. Atmos. Sci.,* **58,** 3312–3327.

——, and ——, 2003: Eddy-zonal flow feedback in the Northern Hemisphere winter. *J. Climate,* **16,** 1212–1227.

Marquardt, D., 1963: An algorithm for least squares estimation of nonlinear parameters. *SIAM J. Appl. Math,* **11,** 431–441.

Panetta, R. L., 1993: Zonal jets in wide baroclinically unstable regions: Persistence and scale selection. *J. Atmos. Sci.,* **50,** 2073–2106.

Swanson, K. L., 2001: Upper-level potential vorticity fluctuations and the dynamical relevance of the time mean. *J. Atmos. Sci.,* **58,** 1815–1826.

Thorncroft, B. J., C. D. Hoskins, and M. E. McIntyre, 1993: Two paradigms of baroclinic-wave life-cycle behavior. *Quart. J. Roy. Meteor. Soc.,* **119,** 17–55.